Proceedings of IMECE'03
2003 ASME International Mechanical Engineering Congress & Exposition
Washington, D.C., November 16-21, 2003

IMECE2003-42393

IN SITU TEMPERATURE DISTRIBUTION MEASUREMENT IN AN OPERATING POLYMER ELECTROLYTE FUEL CELL

Matthew M. Mench,

Daniel J. Burford, and Tyler W. Davis

Electrochemical Engine Center
Department of Mechanical and Nuclear Engineering
Pennsylvania State University
University Park, PA 16802, USA
Tel: +1-814-865-0060
Fax: +1-814-863-4848
e-mail: mmm124@psu.edu

ABSTRACT

The temperature distribution in a polymer electrolyte fuel cell (PEFC) is of critical importance to the water balance, as well as to other kinetic and transport phenomena that are known to be functionally dependent on temperature. However, direct measurement of localized temperature is difficult, due to the two-phase nature of flow in the gas channels and the small through-plane dimensions of a typical electrolyte. To circumvent these difficulties, an array of micro-thermocouples was embedded directly between two 25 μm thick Nafion™ electrolyte sheets of a membrane electrode assembly. The embedded array was used to measure electrolyte temperature as a function of current density and fuel cell flow channel location. For the fuel cell tested with natural convective cooling, a temperature increase in the electrolyte of as much as 15°C is observed for current densities of 1 A/cm^2.

NOMENCLATURE

E	fuel cell voltage,V
E^o	reversible open circuit voltage, V
F	Faraday's constant, 96,487 C/equivalent
G	Gibbs energy, J/kgK
H	Enthalpy, J/kg
i	current density, A/cm^2
i_o	exchange current density, A/cm^2
n	electrons transferred for reaction step, eq./mole
R	universal gas constant, 8.314 J/mol·K
T	temperature, K
q''	waste heat per unit active area, W/cm^2
k	thermal conductivity, W/mK

Greek letters

Δ	delta
α	charge transfer coefficient
ζ	stoichiometric flow ratio

Subscripts

ac	activation polarization of the cathode
c	cathode
cell	fuel cell

INTRODUCTION

One of the most important factors influencing the performance of a polymer electrolyte fuel cell (PEFC) is the water balance. Several modes of water transport are active in a fuel cell, including diffusion through the thin film (15-180 μm) electrolyte, electro-osmotic migration (drag) from the anode to cathode under a potential gradient, vaporization and condensation, two-phase water droplet motion, and water generation at the cathode by the electrochemical reaction. Additionally, the anode and cathode flows are typically humidified to some degree to provide adequate moisture to maintain electrolyte conductivity. For a review of PEFC operation and water management, the reader is referred to reference [1].

At one extreme of the overall fuel cell water balance, if there is excess water not completely removed by cathode reactant flow, it accumulates as liquid, blocking pores of the cathode gas diffusion layer (GDL), and reducing oxygen transport to the cathode. This in turn results in increased concentration polarization. At the other extreme, an excessively dry flow will result in reduced electrolyte water content and thus increased ohmic polarization. The goal of a water management scheme in the PEFC is to maximize the reactive area of the membrane electrode assembly (MEA) not suffering from either excessive drying or flooding.

Complicating the water management strategy is the fact that while PEFC systems can approach an overall efficiency of 50-60%, the inefficiencies manifest as thermal dissipative losses. Waste heat affects the water distribution by increasing temperature and thus the local equilibrium saturation pressure of the gases. At a typical PEFCs operating temperature of 80^{o}C and atmospheric pressure, each 1^{o}C change in temperature results in an approximately 5% change in equilibrium saturation pressure [2]. Thus, even small variations in temperature can dramatically affect optimal inlet humidity values, locations of condensation/vaporization, membrane longevity, and a host of other phenomena. Modeling of the temperature distribution in PEFCs is hindered by relatively unknown thermal transport parameters of various PEFC components, which should be highly anisotropic based on an electrical transport analogy. However, direct measurement of localized temperature is difficult, due to the two-phase nature of flow in the gas channels and the small through-plane dimensions of a typical electrolyte. The motivation for this study is to develop and demonstrate an experimental method to accurately measure the electrolyte temperature of an operating PEFC. This technique can be used to estimate the thermal transport parameters of fuel cell materials, as well as provide a database for detailed computational model validation.

There is limited modeling and experimental work in the area of MEA temperature distribution, and scant experimental data are available. Some available published models which include an energy balance show that the internal temperature rises with current density, and also demonstrate the tremendous impact of temperature change on water management [3-5]. Experimental studies were recently performed to determine the temperature at the electrodes of an operating PEFC [6]. In that study, Teflon™ coated 120 μm K-type thermocouples were embedded at the interface between the anode and cathode catalyst layers and electrolyte. The author notes in this work that the technique used tends to underestimate the true temperature at the measurement location due to various effects.

In the present study, uncoated 50 μm R-type thermocouples were embedded within the electrolyte of a 50 cm^2 superficial active area fuel cell to directly measure electrolyte temperature as a function of current density. Embedding thermocouples within the electrolyte avoids measurement difficulties associated with two-phase flow.

EXPERIMENTAL APPROACH

Figure 1 shows a schematic of the overall system utilized. The 50 cm^2 active area fuel cell (Fuel Cell Technologies, Inc., Albuquerque, New Mexico) was controlled and monitored by an Arbin Instruments (College Station, Texas) fuel cell test stand with twenty-five individual galvanostat/potentiostat channels for current/voltage control and monitoring. The test station automatically controls relative humidity, pressure, stoichiometry, and temperature of anode and cathode reactant flows with MITS Pro version 3.0 software. Fuel cell flow channel plate and reactant flow temperatures were monitored and controlled with an array of T-type thermocouples, cartridge heaters, heat tape, and several PID type controllers. Cartridge heaters are used to achieve the initial 80^{o}C condition in the fuel cell. However, with increasing fuel cell current, the cartridge heater controllers shut down power to the heaters completely, since the measured endplate temperature goes above the 80^{o}C set-point.

For embedded micro-thermocouple temperature measurement, R-type thermocouples were selected for two primary reasons: 1) to

withstand the expected electrolyte internal temperature range (20°C to 120°C), and 2) the noble metal based pure platinum (Pt) and 13% Rhodium (Rh)/87% Pt lead wires used to construct the thermocouples do not oxidize in the acidic environment of the fuel cell electrolyte. During preliminary testing, thermocouple wires of 25 μm and 51 μm diameter were used. The 51 μm diameter lead wires were used for experiments described in this paper, because they were determined to be more robust and more often survived the membrane electrode assembly process, while giving accurate temperature readings and not interfering with fuel cell performance.

Micro-thermocouples were manually placed between two sheets of Nafion™ 111 (25 μm thick) electrolyte material that were catalyzed on one side only (Ion Power, Inc. Bear, Delaware). The carbon-supported platinum loading of the catalyzed side of the electrolyte sheets was 0.5 mg/cm^2. To prepare the embedded thermocouples, the catalyzed side of one half-sheet Nafion™ 111 was placed downward on a sheet of Teflon™, and eight thermocouples were arranged relative to the fuel cell cathode flow path approximately as shown in Figure 2. The other single-sided Nafion™ 111 sheet was then placed on top of the sheet with thermocouples, catalyzed side facing upward. With the thermocouples sandwiched between the two Nafion™ sheets to form an instrumented three-layer membrane electrode assembly (MEA) structure, the MEA was placed in a Carver Model M hot press. The temperature was increased and a static load was applied for some time until the sheets were joined together into a single effective sheet. In this configuration, the micro-thermocouples are embedded between the two sheets of Nafion™ electrolyte, thus electronically isolating them from the electrodes. The total surface area of the exposed micro-thermocouple wires in the electrolyte is ~0.02% of the total catalyst area; hence electrochemical reaction with hydrogen/oxygen crossover gas at the wire surface can be effectively neglected.

Membranes have been successfully instrumented with up to eight micro-thermocouples, and electrolyte half-sheet thicknesses used have ranged from 25 μm to 127 μm. The MEA preparation technique does not typically cause damage to the membrane. Most importantly, there is no tearing or break through issue with embedded thermocouples for any of the electrolyte sheet sizes used. Performance with the embedded thermocouples is not significantly affected by the thermocouples, as shown in Figure 3, a polarization curve for a Nafion™ 112 equivalent electrolyte (~50 μm thick) instrumented with eight embedded micro-thermocouples. The fact that open circuit potential (OCP) and overall performance is slightly less than expected for this MEA may indicate slightly increased H_2 crossover. Work is ongoing to quantify and compare the H_2 crossover and performance of these instrumented MEAs to that with off-the shelf Nafion™ 112 MEAs.

The fuel cell was assembled with the instrumented MEA the same way as with a non-instrumented MEA. An incompressible Teflon™ gasket was used for sealing, and single-sided (410 ± 60 μm thick) uncatalyzed ELAT® (E-TEK Div. of De Nora N.A., Inc. Somerset, New Jersey) was used as the GDL on both electrodes. After cell assembly, the lead wires from the R-type thermocouples were soldered to high-grade copper extension wire, connecting the embedded thermocouples to the National Instruments SCXI 1000 chassis with NI 1303 terminal block DAQ system with built-in cold-junction compensation thermistor. To ensure accurate temperature readings, raw data were calibrated to a steady state temperature of 80°C by maintaining the fuel cell backing plate and associated flows at 80°C for about 30 minutes at open circuit conditions.

RESULTS AND DISCUSSION

For the test results reported, only three of the eight original micro thermocouples gave reliable output. Four were damaged during MEA or cell assembly, and a fifth thermocouple gave inaccurate results due to a twisted wire that resulted in dual thermocouple junctions, as determined from post test *ex situ* microscopic examination. A much greater yield fraction of functioning thermocouples (~80%) has since been achieved in subsequent MEAs following assembly procedure modification. The locations of the thermocouples that functioned correspond to locations number 3, 7, and 8 in Figure 2. Locations 3, 7, and 8 are located at approximately 20, 90, and 95% of the fractional distance along the cathode flow path from inlet to exit (x/L), respectively. Post-test *ex situ* microscopic examination was used to determine the fractional location of the thermocouple bead along the cathode flow path.

A standard operating state was utilized for testing; conditions are shown in Table 1 for reference. The cell was operated at an initially constant fuel cell flowfield plate temperature of 80°C (although this increased during testing due to heat generation), both anode and

cathode were fully humidified to 80°C, the absolute pressure for both anode and cathode was 151,987 Pa (1.5 atm), and the stoichiometries of the anode (ζ_a) and cathode (ζ_c) were held constant at 1.2 and 2.0, respectively. A polarization curve showing the performance of the MEA at these conditions is shown in Figure 3.

Figure 4 shows the measured electrolyte temperature versus time trajectory, as current density was varied in discrete increments. The results in Figure 4 were determined by initiating testing at open circuit potential (OCP) at steady-state, then increasing the current density in 0.1 A/cm^2 increments at regular intervals to allow the fuel cell to reach steady state. A transient response occurred immediately following current density step variation. It should be noted that this dynamic response is a result of increasing current, as well as the adjustment of the control system to achieve the new flow rate corresponding to the chosen stoichiometry. It can be seen that the temperature at each location increases with current density, as expected. As current density increases, fuel cell efficiency (cell voltage) decreases, and thus waste heat increases. The thermal heat generation flux per unit active area of the fuel cell can be shown as [7]:

$$q'' = -i\left(\frac{\Delta H}{nF} + E_{cell}\right) \quad (1)$$

where i is the operating current density, ΔH is the enthalpy change due to reaction, and E_{cell} is the fuel cell operating voltage. Therefore, as current density increases (corresponding also to reduced cell voltage), the thermal energy dissipation flux, and thus internal temperature is expected to increase unless other modes such as latent heat of vaporization or heat removal from process flow increase an equivalent amount.

Figure 5 shows the average measured electrolyte temperature as a function of current density. In this plot, the average temperature at each current density from Figure 4 was taken to provide a more clear view of the temperature rise in the electrolyte. It should be noted that, although the embedded thermocouples are in the middle of the thin electrolyte, there is expected to be a temperature distribution within the electrolyte itself. This is a result of the fact that a majority of the activation overpotential is associated with the cathodic oxidation reduction reaction (ORR) when operating on pure hydrogen. Therefore, the highest local temperature is expected at the cathode catalyst layer, not in the middle of the electrolyte.

Figure 6 shows a plot of the absolute change in local temperature compared to OPC temperature (ΔT) versus current density (i). The temperature difference is quite large, up to 15°C at 1 A/cm^2 at x/L = 0.95 (corresponding to 95% of the path length from cathode inlet to exit). The through-plane thermal resistance of the polymer electrolyte and relatively thick (410 ± 60 μm) gas diffusion layer is expected to be relatively high compared to the thermal resistance of the metal flow field plates, contributing to the measured temperature rise. Thinner GDLs will have reduced thermal transport resistance, proportional to thickness. It is therefore apparent that intelligent design of the GDL and electrolyte for controlled thermal transport is desired to prevent excess heat buildup and internal temperatures that can greatly affect water management, flooding location, membrane durability, and various other transport and electrochemical phenomena functionally related to temperature.

For the given test conditions, the temperature change in the electrolyte follows a steadily increasing relationship with current density, as can be seen in Figure 6. For current densities over 1 A/cm^2, the relationship between ΔT and current density goes through a transition and follows a seemingly asymptotic approach to a maximum ΔT. This rollover to asymptotic behavior may be due to natural convective effects from the test cell. At the rollover point, the cell power is approximately 0.55 W/cm^2, or 27.5 W. Assuming a reasonable natural convection coefficient of 2 W/cm^{2}K, this amount of waste heat could easily be dissipated by the fuel cell. Also, the additional energy required for latent heat of vaporization could be a factor at high current densities where flooding is expected. Both phenomena may play a role, and much more work needs to be done to understand this phenomena. It should be noted that the thermocouples were calibrated at operating temperature of 80°C, and thus should accurately represent the true internal temperature to ± 1°C.

From Figure 6, it appears that from 0 to 0.7 A/cm^2, the thermocouple located at the upstream at 20% along the cathode triple serpentine path was a few degrees warmer than locations at 90 and 95% along the cathode flow path, respectively. At higher current densities, the trend is reversed and the downstream locations are warmer by a few degrees. It is difficult to make a definitive

conclusion based on this single data set, but the switch could be a result of the fact that downstream locations would have increased concentration polarization and heat generation due to reactant depletion or flooding. At lower bulk cell current densities, the local current density at the inlet can be higher [8], increasing heat generation and temperature. It should be noted that the majority of this crossover trend occurs within the thermocouple error ranges, and more analysis needs to be completed before any definitive conclusion can be reached.

To interpret these results, it is important to note that the boundary conditions of this laboratory test cell are different from a commercial stack, where active channel cooling is typically used. This may explain some of the differences between laboratory and stack data at similar operating conditions, and illustrates the importance of maintaining a stable laboratory environment to ensure valid comparison of results. Nevertheless, this technique can be applied to full-size stacks, and mapping of many different fuel cell configurations can be accomplished. The results presented also demonstrate that use of an isothermal assumption in calculations may not be accurate at moderate to high current densities.

Anticipated Temperature Rise

It has been shown that as the current density increases, the thermal dissipation also increases. Thus, the temperature within the electrolyte should also increase with current density unless latent heat of vaporization, convection from the cell, heat loss via process flow or another phenomenon compensates for this increase. It is desirable to know the expected functional dependency of electrolyte temperature on current. The following section presents a basic estimation of this relationship. The cell voltage can be estimated as:

$$E_{\text{cell}} = E^o - |\eta_{ac}| - \eta_r = -\frac{\Delta G}{nF} - |\eta_{ac}| - \eta_r \qquad (2)$$

where η_{ac} represents the activation overpotential at the cathode, and η_{r} represents the total ohmic loss including all cell components. E^o is the open circuit potential (OCP) determined from thermodynamics (1.18 V at 80°C), and concentration and anode activation polarizations are neglected. This is reasonable for relatively high stoichiometry operation on pure hydrogen. The actual cell OCP is less than the theoretical OCP, and is a function of hydrogen permeation through the electrolyte and other factors that can be included in the cathode polarization term, but for the purpose of this analysis can be treated as a constant. Because the cathode suffers relatively high activation polarization, a Tafel relationship can be used [9]:

$$\eta_{ac} = \frac{\mathrm{RT}}{n\mathrm{F}\alpha}\ln\left(\frac{i}{i_o}\right)\Bigg|_c \qquad (3)$$

where i_{o} is the cathodic exchange current density, α is the charge transfer coefficient (representing the fraction of overpotential that is utilized in the cathodic reaction at the electrode – assumed to be 1.0), n is the number of exchange electrons in the elementary reaction (assumed to be 1.0), and other symbols are defined in the Nomenclature Section. Substituting Eqns. (2-3) into Eq. (1) yields:

$$q'' = -i\left[\frac{\Delta H}{nF} - \frac{\Delta G}{nF} - \frac{\mathrm{RT}}{n\mathrm{F}\alpha}\ln\left(\frac{i}{i_o}\right)\Bigg|_c - i\sum_{k=1}^{n} r_k\right] = \\ + i^2\sum_{k=1}^{n} r_k + i\frac{\mathrm{RT}}{n\mathrm{F}\alpha}\ln\left(\frac{i}{i_o}\right) - i\frac{T\Delta S}{nF} \qquad (4)$$

where r_k represents the ohmic resistance of each component k in the fuel cell. For proper fuel cell design, this resistive term is dominated by the ohmic drop for ionic transfer through the electrolyte. The first term on the right hand side of Eq. (4) mainly represents the ohmic dissipation within the electrolyte, and is an i^2r relationship, as expected. The second term of Eq. (4) represents the heat flux generated by activation polarization in the cathode catalyst layer. The third term in Eq. (4) is a linearly varying function of current density and represents the sum of the Peltier heat generated at each electrode. The functional relationship derived in Eq. (4) is shown in Figure 7, a plot of calculated ohmic and cathode activation polarization as a function of current density. Since the third term in Eq. (4) is linearly related to the heat generation, it is not included in Fig. 7. The ionic conductivity for the electrolyte was chosen to be 0.1 S/cm, based on the assumption of a fully humidified membrane in contact with vapor-phase water [10]. The heat flux generation of Eq. (4) is also shown on Figure 7. This plot should be viewed only as a guide to the expected qualitative behavior of the heat generation with current density, given the limiting assumptions made. Since the activation polarization becomes linear with increasing current density similar to ohmic losses, the heat generation per active area can be fit well by a second order

polynomial, with the squared term equivalent to the combined ohmic and activation components, and the linear term functionally equivalent to the third term in Eq. (4). The qualitative shape of this result is demonstrated from the experimental data at low current density.

The functional dependence of the heat generation in Eq. (4) can be expressed by the dominating term as:

$$q'' \propto i^2 r \tag{5}$$

where r represents the total resistance (electronic and ionic) within the fuel cell. At the interface between the GDL and the reactant channels, heat transfer by convection will take place. However, within the GDL and electrolyte, conduction dominates. From Fourier's Law of heat conduction, the relationship between the heat flux generated and the temperature difference across the through-plane thickness of the electrolyte and gas diffusion layers (GDLs) is as follows:

$$q'' = -k\frac{\Delta T}{\Delta x} \text{ , therefore } q'' \propto \Delta T \tag{6}$$

Therefore ΔT with current density should follow the functional form of Eq. (4), until other phenomena not accounted for in Eq. (6) affect heat transfer – e.g. phase change or convective heat loss. Combining Eq. (5-6) yields a functional relationship between current density and change in temperature, valid for a limited set of assumptions discussed:

$$q'' \propto i^2 r \propto \Delta T \tag{7}$$

CONCLUSIONS

Knowledge of temperature distribution within an operating fuel cell is critical for proper water management as well as fundamental understanding and modeling of various other phenomena. In this work, a novel method for precise real time measurement of the electrolyte temperature in an operating PEFC with embedded micro-thermocouples has been implemented. The following conclusions can be made regarding this work:

1) Temperature variations in 50 cm^2 fuel cell with a 50 μm thick electrolyte were shown to be greater than 15°C for currents > 1 A/cm^2, indicating a traditionally used isothermal assumption may not be accurate enough for modeling purposes. This high value of temperature change is a result of material properties and the natural convective boundary condition for this laboratory fuel cell, and may explain some differences between laboratory and stack data, where heat transfer boundary conditions are very different.
2) The results of this work indicate the critical role that fuel cell materials play in the determination of the temperature gradient, and that careful quantification and tailoring of the thermal transport parameters is a necessary step for achieving optimal design.
3) For the fuel cell used, electrolyte temperature increases can be accurately fit with a second order polynomial up to a current density of around 1 A/cm^2. Once a current density of 1 A/cm^2 is surpassed, the rise in temperature of the electrolyte transitions to asymptotic behavior. It is presumed that this change in the temperature-current relationship is due to convective heat loss from the insinuated test cell, or latent heat effects, and is not a universal event for all fuel cells.

Finally, it should be noted that there is much ongoing work being done to fully characterize and understand the temperature distribution in a PEFC as a function of various parameters using the embedded micro-thermocouple technique presented in this work, including examination of the relative errors and repeatability of data collection.

ACKNOWLEDGEMENTS

This project was supported in part by a graduate fellowship from the National Science Foundation.

REFERENCES

1. Larminie, J. and Dicks, A., 2003, *Fuel Cell Systems Explained*, 2nd Edition, John Wiley and Sons, Ltd., Chichester, United Kingdom.
2. Moran, M. J. and Shapiro, H. N., 1995, *Fundamentals of Engineering Thermodynamics*, John Wiley and Sons, Ltd., New York.
3. Kudriavtsev, V., and Das, R., 2002, "Three-dimensional Modeling of a Medium Size PEM Fuel Cell Stack: Thermal Effects and Electrical Performance," *Proceeding of 4th International Symposium on Computational Technologies for Flow/Thermal/Chemical Systems with Industrial Applications*, August 4-8, BC, Canada.

4. Lee, W-k., Shimpalee, S., and Van Zee, J.W., 2003, "Verifying Predictions of Water and Current Distributions in a Serpentine Flow Field Polymer Electrolyte Membrane Fuel Cell," *J. Electrochem. Soc.*, Vol. 150, pp. A341-A348.
5. Natarajan, D., and Nguyen, T.V., 2003, "Three-dimensional Effects of Liquid Water Flooding in the Cathode of a PEM Fuel Cell," *J. Power Sources*, Vol. 115, pp. 66-80.
6. Vie, P. J. S., 2002, "Characterization and Optimization of the Polymer Electrolyte Fuel Cell," *Ph.D. Thesis, NTN University*, Trondheim, Norway.
7. Divisek, J., 2003, "Low Temperature Fuel Cells," Chapter 9 in *Handbook of Fuel Cells-Fundamentals*, *Technology and Applications*, W. Vielstich, A. Lamm, and H. A. Gasteiger, Eds., Vol. 1, John Wiley and Sons, Ltd., Chichester, United Kingdom.
8. Mench, M. M., Wang, C. Y., and Ishikawa, M., 2003, "*In situ* Current Distribution Measurements in Polymer Electrolyte Fuel Cells," *J. of Electrochem. Soc.* Vol. 150, pp. ppA1052-A1059.
9. Bard, A. J., and Faulkner, L. R., 2002, *Electrochemical Methods-Fundamentals and Applications*, 2nd Edition, John Wiley and Sons, Inc., New York.
10. Springer, T. E., Wilson, M. S., and Gottesfeld, S., 1991, "Polymer Electrolyte Fuel Cell Model," *J. Electrochem. Soc.*, Vol. 136, pp. 2334-2342.

Table 1. Baseline Operating Conditions

Parameter	Value	Units
Electrolyte	Two joined Nafion 111 (25 μm) sheets (E.I. du Pont de Nemours and Company)	NA
Gas diffusion layer	ELAT® (E-TEK of De Nora North America) anode and cathode	NA
Catalyst loading (carbon supported)	0.5	mg/cm^2
Cell temperature	80	^oC
Anode inlet dew point temperature	80	^oC
Cathode inlet dew point temperature	80	^oC
Anode/Cathode back pressure	151,987 (1.5)	Pa (atm)
ζ_a	1.2	1
ζ_c	2.0	1
Anode gas	Ultra high purity H_2 (>99.999 %)	NA
Cathode gas	Commercial air (79% N_2, 21% O_2)	NA

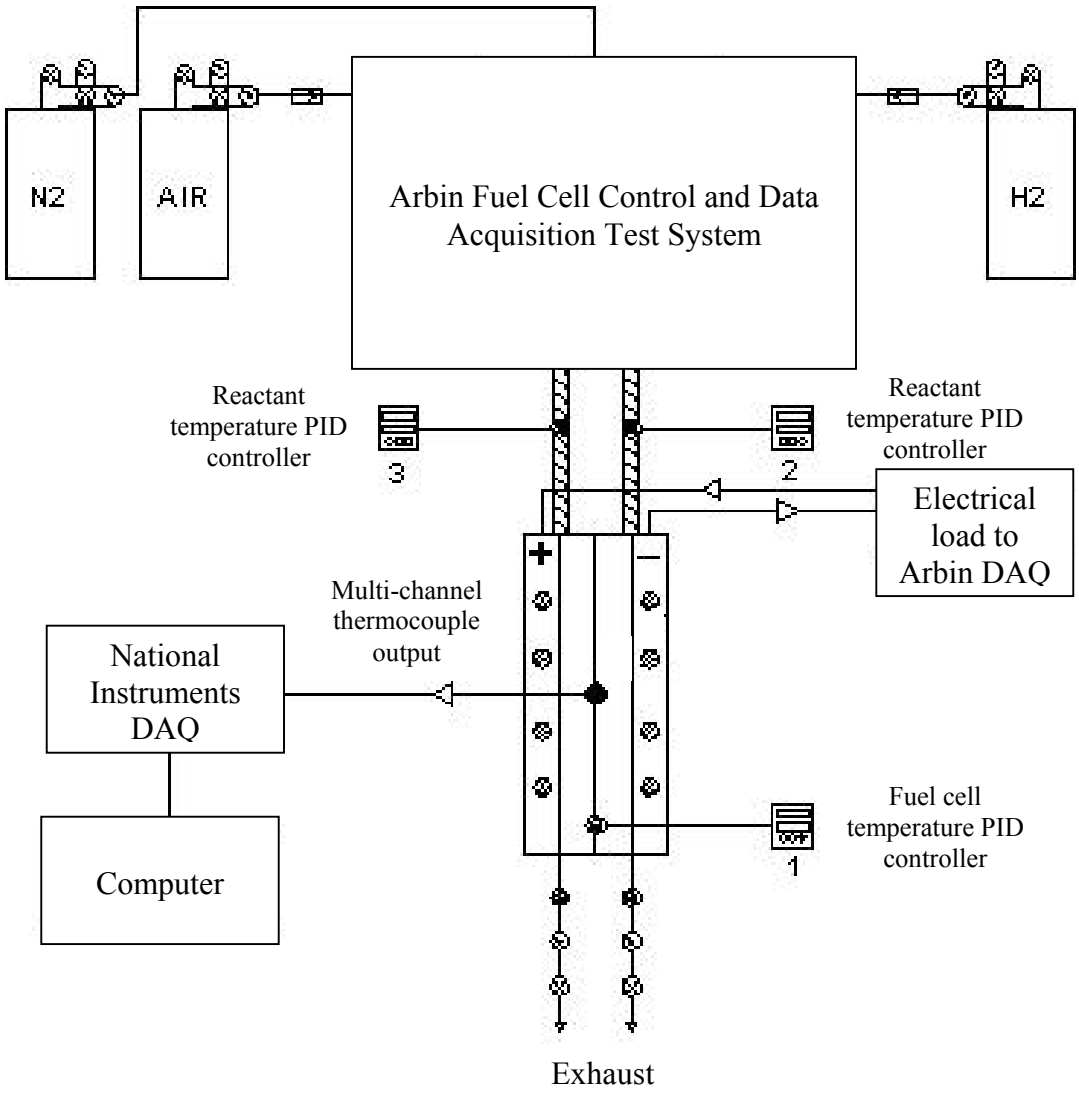

Figure 1. Schematic of experimental test system used for *in situ* temperature distribution measurement.

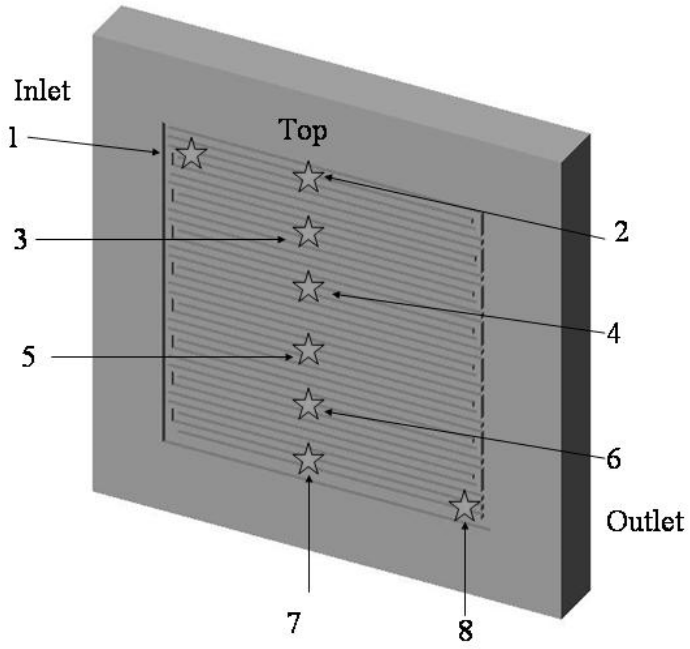

Figure 2. Schematic of approximate thermocouple bead placement in 50 cm^2 fuel cell.

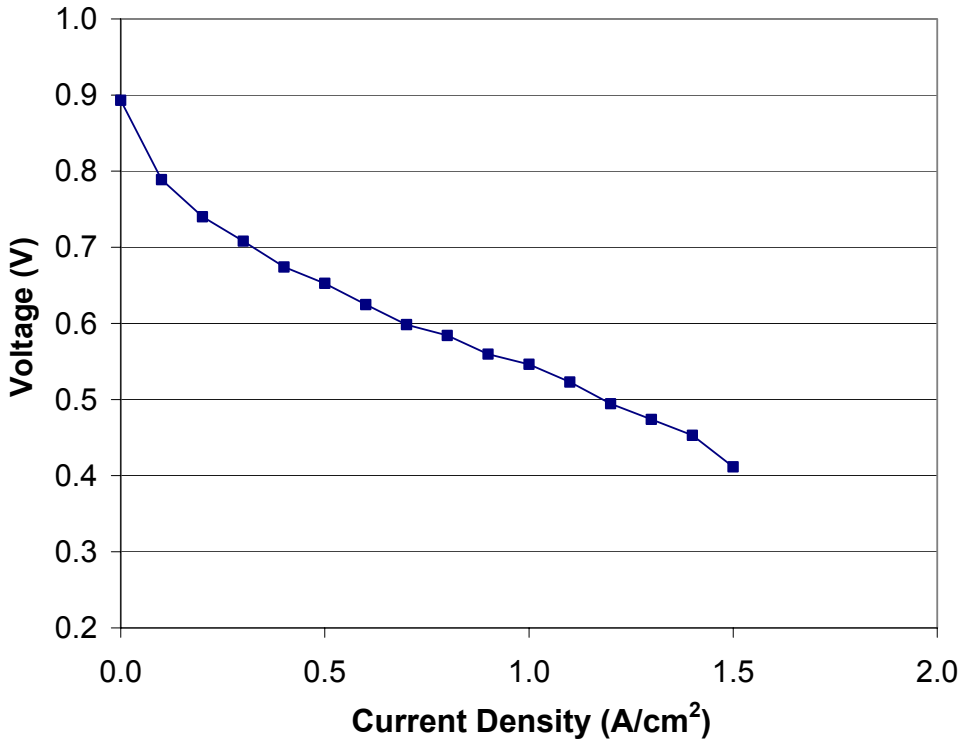

Figure 3. Performance of PEFC with eight embedded micro-thermocouples between two 25 μm Nafion™ sheets (Nafion 112 equivalent MEA). Pressure A/C = 1.5 atm, 100% relative humidity at 80°C air cathode, 100% relative humidity at 80°C H_2 anode, ζ_c = 2.0; ζ_a = 1.2, T_{cell} = 80°C.

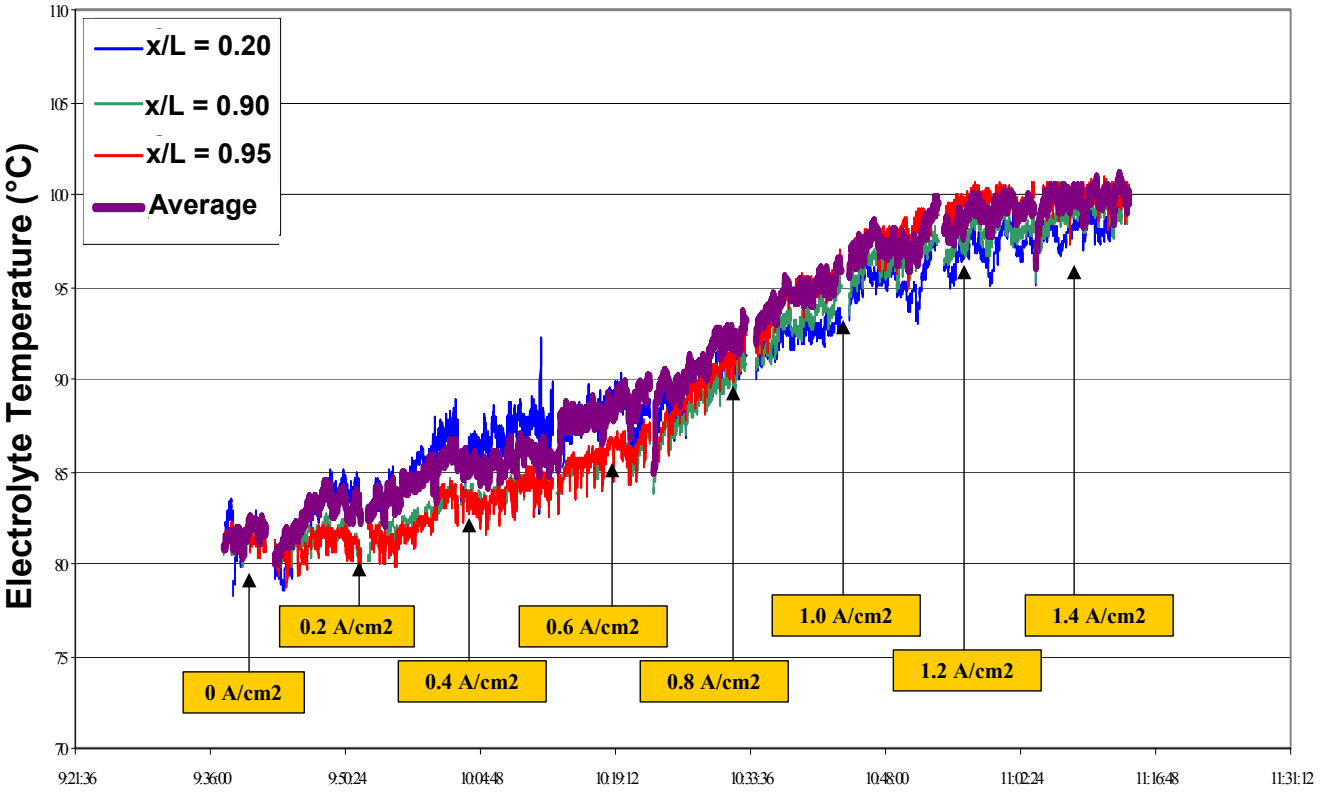

Figure 4. Temperature increase with current density recorded with embedded micro thermocouples. x/L refers to the fractional location of the thermocouple bead along the cathode flow channel. Pressure A/C = 1.5 atm, 100% relative humidity at 80°C air cathode, 100% relative humidity at 80°C H_2 anode, ζ_c = 2.0; ζ_a = 1.2, T_{cell} = 80°C.

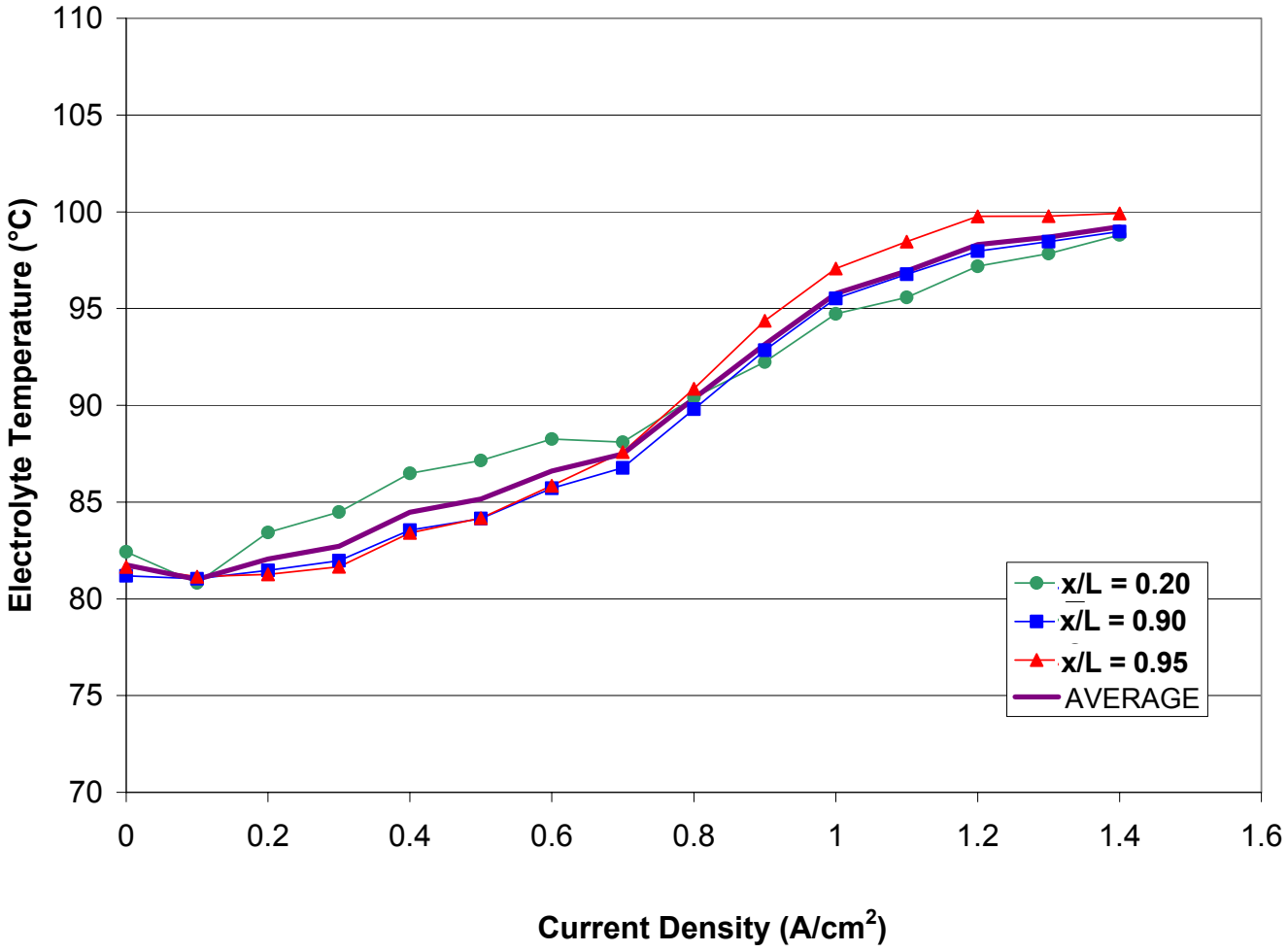

Figure 5. Average electrolyte temperature at various locations as a function of current density. Pressure A/C = 1.5 atm, 100% relative humidity at 80°C air cathode, 100% relative humidity at 80°C H_2 anode, ζ_c = 2.0; ζ_a = 1.2, T_{cell} = 80°C.

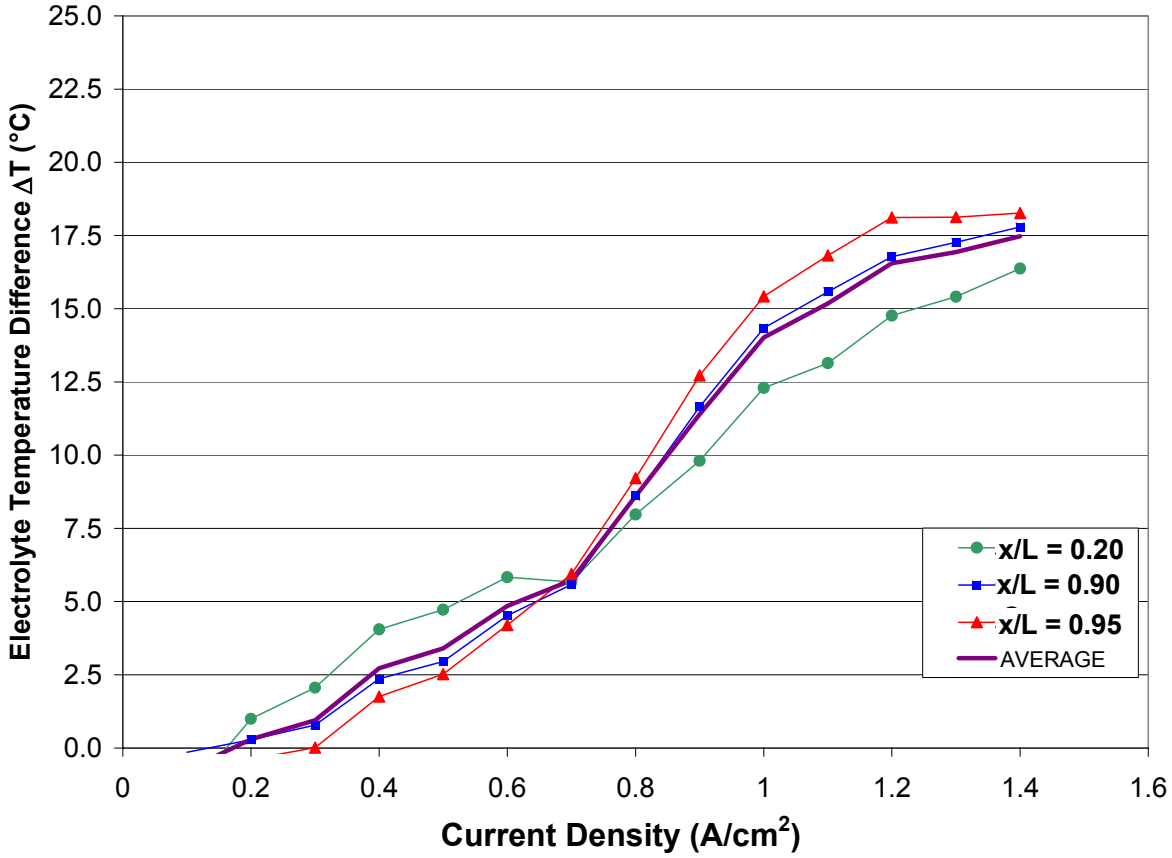

Figure 6. Difference between initial electrolyte temperature at open circuit conditions and electrolyte temperature as function of current density. Pressure A/C = 1.5 atm, 100% relative humidity at 80°C air cathode, 100% relative humidity at 80°C H_2 anode, ζ_c = 2.0; ζ_a = 1.2, T_{cell} = 80°C.

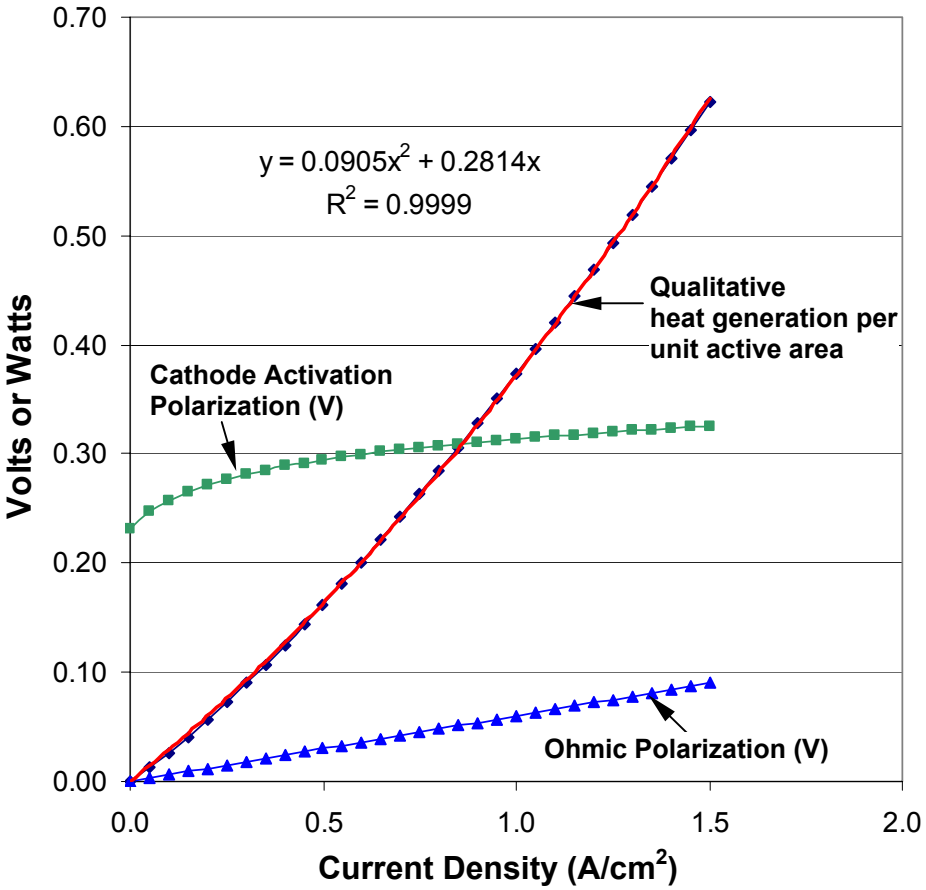

Figure 7. Calculated ohmic and cathode activation polarization as a function of current density and heat generation per unit active area.